

CMOS-Based Phase Fluorometric Oxygen Sensor System

Vamsy P. Chodavarapu, *Student Member, IEEE*, Daniil O. Shubin, Rachel M. Bukowski, Albert H. Titus, *Member, IEEE*, Alexander N. Cartwright, *Member, IEEE*, and Frank V. Bright

Abstract—The design and development of a phase fluorometric oxygen (O_2) sensor system using single-chip CMOS detection and processing integrated circuit (DPIC) and sol-gel derived xerogel thin-film sensor elements is described. The sensor system determines analyte concentrations using the excited state lifetime measurements of an O_2 -sensitive luminophore (tris(4,7-diphenyl-1,10-phenanthroline)ruthenium (II)) embedded in the xerogel matrix. A light emitting diode (LED) is used as the excitation source, and the fluorescence is detected by the DPIC using a 16×16 phototransistor array on-chip. The DPIC also consists of a current mirror, current-to-voltage converter, amplifier, bandpass filter, and phase detector. The DPIC output is a dc voltage that corresponds to the detected fluorescence phase shift. With a 14-kHz modulation frequency, the entire system including driving the LED consumes 80 mW of average power. The sensor system provides stable, reproducible, analytically reliable, and fast response (~ 20 s) to changes in the gaseous oxygen concentrations and establishes the viability for low cost, low power and miniaturized biochemical sensor systems.

Index Terms—Chemical sensor, CMOS, frequency response, lifetime sensors, oxygen sensor, phase angle, phase fluorometry, phototransistor, sensor integration, signal processing, sol-gel, VLSI, wavelength response, xerogel.

I. INTRODUCTION

OXYGEN (O_2) sensors play an important role in various biochemical, food and beverage, and environmental applications [1]. In general, optical O_2 sensors are more attractive than conventional amperometric devices, such as Clark electrodes (CEs), because optical sensors do not consume O_2 , are not easily poisoned by sample constituents, and have fast response characteristics [2]–[4]. Following recent trends in the sensor technologies, there is a growing demand for sensors that are low cost, low power, miniaturized, and easily mass producible [5], [6]. Many of the above listed features can be achieved by the use of standard CMOS (complementary metal oxide semi-conductor) technologies for the development

of monolithically integrated detection and signal processing components that form an essential part of an optical sensor system [7], [8].

Over the past several years, we [9]–[14] and others [15]–[18] have been developing sol-gel derived xerogel platforms for O_2 sensing. Xerogels are nanostructured porous glasses that are produced under ambient conditions. Xerogels have several advantages including good thermal stability, tunable sensitivity, and optical transparency. Also xerogels can be used for sequestering a wide variety of active agents (e.g., luminophores) within their porous structures [19]. Typically, optical O_2 sensors operate on the measurement of the luminescence intensity [11], [20] or lifetime [14], [21], [22] of active agents like ((tris(4,7-diphenyl-1,10-phenanthroline) ruthenium(II), ($[Ru(dpp)_3]^{2+}$)) sequestered within the xerogel architecture. Intensity measurements are typically made using a steady-state optical excitation source [for example, an light emitting diode (LED) with a constant bias]; the signal of interest is then the intensity of the luminescence from the luminophores. The presence or absence of the analyte of interest will then cause the luminescence intensity to increase or decrease. Lifetime measurements require the optical excitation source to be modulated, producing a modulated luminescence signal. The luminescent signal will have a phase shift relative to the excitation signal that can be measured and related to the lifetime, which can then be related to analyte concentration.

Optical O_2 sensors based on the measurement of the luminescence lifetime can be more attractive in comparison to those based on the measurement of intensity for several reasons including: 1) minimal susceptibility to light source (stimulation) and detector drift; 2) insensitivity to changes in optical path; 3) insensitivity to drift due to luminophore degradation and/or leaching. However, the direct measurement of the luminophore excited state lifetimes of the luminophores can necessitate elaborate signal detection and processing instrumentation when performed in the time domain because the lifetimes are relatively short [23]. Phase fluorometry is an alternative to time-domain methods that is realistically simple and requires less effort in the development of the signal detection and processing instrumentation [22], [24]. In this approach, the sample is excited with sinusoidal modulated light and the phase shift between the excitation and the luminescence is measured [25].

Previously, we demonstrated the feasibility of developing luminescence intensity based O_2 sensors systems by using CMOS photodetectors and xerogel thin-film sensor elements [26]–[28]. In the current work, we demonstrate the first example of an integrated phase fluorometric sensor *system* using xerogel sensor

Manuscript received January 30, 2006; revised August 21, 2006. This work was supported by the Johnson & Johnson Focused Giving Program and the National Science Foundation. This paper was recommended by Guest Editor D. Wilson.

V. P. Chodavarapu, A. H. Titus, and A. N. Cartwright are with the Department of Electrical Engineering, University at Buffalo, The State University of New York, Buffalo, NY 14260 USA (e-mail: ahtitus@eng.buffalo.edu).

D. O. Shubin is with the Department of Electrical Engineering, University at Buffalo, The State University of New York, Buffalo, NY 14260 USA. He is now with General Electric Global Research, Niskayuna, NY 12309 USA.

R. M. Bukowski and F. V. Bright are with the Department of Chemistry, Natural Sciences Complex, University at Buffalo, The State University of New York, Buffalo, NY 14260 USA.

Digital Object Identifier 10.1109/TCSI.2006.888680

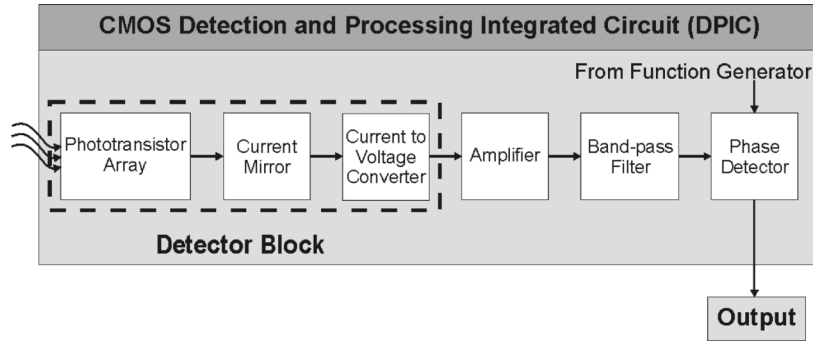


Fig. 1. Simplified block diagram of DPIC.

elements in concert with a novel single-chip CMOS detection and processing integrated circuit (DPIC). There are previously published works by us [29] and other groups [22], [24] which describe related low cost integrated systems using CMOS and/or volume production signal processing components. However, all previous systems are based on discrete components that consume much more power in comparison to our DPIC system. Moreover, all previous systems used external detectors such as silicon photodiodes and thus have limited options for miniaturization.

Fig. 1 shows the simplified DPIC block diagram. In the current article, we describe the essential parameters that are to be considered in the development of these sensor systems including the photodetector design, factors limiting the operating frequency, and factors that influence the sensor system sensitivity. Section II provides the essential background of luminescence quenching and the description of the Stern–Volmer intensity and lifetime equations which form the basis of luminescence based sensor systems. Section III describes the procedure for fabricating the xerogel based sensor elements. Section IV describes the DPIC design and component development. Finally, Section V describes the experimental setup and the preliminary results detailing the system performance as an O_2 sensor.

II. BACKGROUND

In the simplest scenario, we assume all the luminophore molecules are equally accessible to the O_2 molecules (a generally acceptable assumption), so luminophore quenching by O_2 can be described by the Stern–Volmer equations [25]

$$\frac{I_0}{I} = \frac{\tau_0}{\tau} = 1 + K_{SV}[O_2] = 1 + K_q\tau_0[O_2] \quad (1)$$

where I_0 and τ_0 are the luminescence intensity or lifetime in the absence of O_2 respectively, I and τ are intensity or lifetime in the presence O_2 respectively, K_{SV} is the Stern–Volmer constant, k_q is the bimolecular quenching constant and $[O_2]$ is the fractional gaseous O_2 concentration.

In phase fluorometry, the method employed in our sensor system, the luminophore is excited with a sinusoidally modulated light with a modulation frequency, f . The resulting emission is at the same frequency, but is phase shifted, θ , with respect

to the excitation and the extent of the phase shift depends on the luminophore excited state lifetime (τ) [25]

$$\tan(\theta) = (2\pi f) * \tau. \quad (2)$$

Therefore, from (1) and (2), measurements of the phase shift, θ provides a convenient way to monitor analyte/quencher concentrations.

III. XEROGEL SENSOR FILM FABRICATION

A. Reagents and Materials

The following reagents are used: tris(4,7'-diphenyl-1-10'-phenanthroline) ruthenium(II) chloride pentahydrate ($[Ru(dpp)_3]Cl_2 \bullet 5H_2O$) (GFS Chemicals); tetraethoxysilane (TEOS), and *n*-octyltriethoxysilane (C8-TEOS); HCl (Fisher Scientific); and ethanol (EtOH) (Quantum Chemical). $[Ru(dpp)_3]^{2+}$ is purified as described in the literature [30]. All other reagents are used as received. All aqueous solutions are prepared with deionized water that has been treated with a Barnstead NANOpure II system to a specific resistivity of $17.7M\Omega \bullet cm$. Standard glass microscope slides (Fisher Scientific Co.) are used as the xerogel film substrate.

B. Preparation of O_2 Sensor Films

The sol stock solution is prepared by physically mixing 0.513 mL of C8-TEOS, 0.362 mL of TEOS, 0.625 mL of EtOH, and 0.200 mL of 0.1-M HCl in deionized water. The stock solution is sonicated for 1 h under ambient conditions. Glass microscope slides are cut into 25 mm \times 25 mm pieces, and cleaned using the following protocol: 1) 15 min soaking in acetone; 2) wash with copious amounts of deionized water; 3) 1 h soaking in 1-M NaOH; 4) wash with copious amounts of deionized water; 5) 1 h soaking in 1 M HCl; 6) wash with copious amounts of deionized water; 7) dry slides in an oven at 70 °C for 1 h. To fabricate the O_2 -responsive sensor films an 80- μ L aliquot of the stock solution is physically mixed with a 20- μ L aliquot of 12.5 mM $[Ru(dpp)_3]^{2+}/EtOH$. An 80- μ L aliquot of this doped sol mixture is then pipetted onto a clean glass microscope slide. The resulting film is allowed to age in the dark at room temperature for ten days before testing.

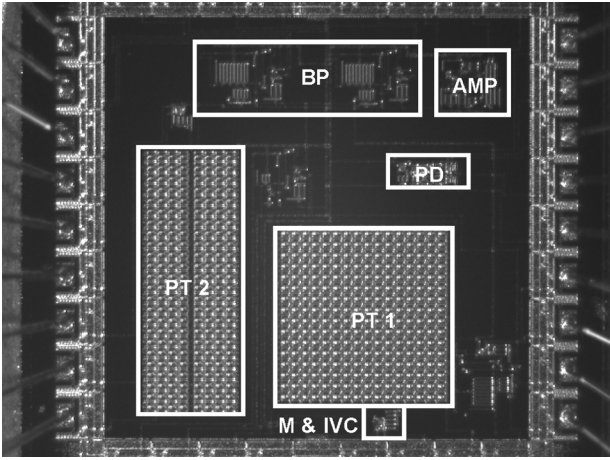


Fig. 2. Microphotograph of DPIC; PT1: square phototransistor (used in the current work); PT2: rectangular phototransistor; M and I-VC: current mirror and current-to-voltage converter; AMP: amplifier; BP: bandpass filter; PD: phase detector.

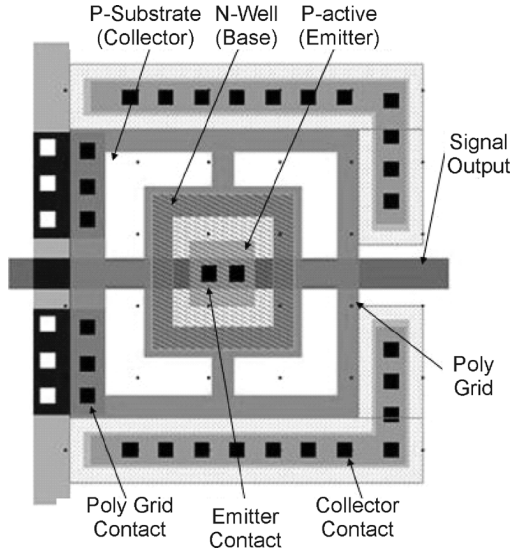


Fig. 3. Layout of one phototransistor pixel. The dimensions of the entire structure shown is $40.8 \mu\text{m} \times 40.8 \mu\text{m}$.

IV. DPIC SYSTEM DESCRIPTION AND COMPONENT CHARACTERIZATION

The $2.2 \text{ mm} \times 2.2 \text{ mm}$ DPIC is fabricated using the AMI $1.5 \mu\text{m}$ CMOS process available through MOSIS [31]. Fig. 2 is a microphotograph of the DPIC. The DPIC consists of phototransistor array (PT1 in Fig. 2), current mirror, current-to-voltage converter, amplifier, bandpass filter, and phase detector. A few off-chip passive devices are also required, and will be described later.

A. Detector Block

The 16×16 phototransistor array measures $720 \mu\text{m} \times 720 \mu\text{m}$. Fig. 3 shows the layout of a phototransistor pixel. The vertical phototransistor is formed by the p-active (emitter)/n-well (base)/p-substrate (collector), and has one of the highest responsivities of the photodetectors available in this standard CMOS process [26], [28]. The polysilicon grid shown in Fig. 3 covers

the n-well (base) to form a ring around the p-substrate (collector) contact. The polysilicon grid is set to the highest potential (5 V within our system) to increase the depletion region where the photogenerated carriers can be easily swept toward the p-active region (emitter). The phototransistor produces currents that are about 100 to 1000 times larger in comparison to a comparably sized photodiode. However, the tradeoff is a bandwidth in the range of few hundred kilohertz compared to the megahertz or higher bandwidth of a photodiode.

Fig. 4 shows the detector block circuit diagram with the phototransistor array, current mirror, and current-to-voltage converter. The vertical phototransistor can only be used in an emitter-follower configuration, converting the input optical signal to an output electrical current signal. For very low current levels, such as those resulting from LED-based fluorescence sensors, real-time current amplification is required; a simple current mirror can be used for this task, as implemented by the transistors (P1-P5). In our system, the current gain is set to 10 A/A, and thus I_{Photo} is amplified to I_{Total} . The amplified current, I_{Total} , is then converted into a voltage, V_{node} , by using a linear current-to-voltage converter formed by the transistors (P6-P7, N1-N2). The linear current-to-voltage converter is based upon the channel length modulation effect in short-channel devices [32]. The current-to-voltage converter output drives the common-source amplifier implemented by P8 and N3 which produces an output voltage, V_{out} .

The detector block operation is as follows: an increase in the intensity of the optical signal on the phototransistor causes an increase in I_{Photo} which causes an increase in I_{Total} . Since, N1 and N2 are biased at a fixed gate-to-source voltage, V_{bias1} , an increase in I_{Total} causes the drain current through P6 to decrease. The current through P6 is mirrored to P7, and the decrease in the drain current through P7 causes V_{node} , the drain-to-source voltage of N2, to decrease because the gate-to-source voltage of N2 is fixed at V_{bias1} . A decrease in the value of V_{node} causes V_{out} to increase concomitantly.

Fig. 5 illustrates the measured detector responsivity as a function of wavelength obtained by recording V_{node} from the detector system at a known wavelength and light fluence. A xenon arc lamp served as the white light source and a monochromator (Acton Research, Model: SpectraPro 2300i) with a full width at half max (FWHM) bandpass of 4 nm was used to control the wavelength. The optical power impinging upon the detector is measured using an optical power meter (Coherent, Model: Fieldmaster K538). Our new detector system exhibits an analytical useful wavelength response from 475 nm to at least 675 nm (note that the absorption coefficient for Si drops significantly for wavelengths greater than 690 nm [33]) The average responsivity is $\sim 35 \text{ V}/\mu\text{W}$ near 600 nm; the $[\text{Ru}(\text{dpp})_3]^{2+}$ emission maximum. At 675 nm, the responsivity peaks above $45 \text{ V}/\mu\text{W}$, which indicates the wavelength that provides the largest output signal for a given optical input power. Our xerogel emits at a fixed wavelength (around 595 nm), so clearly a different luminophore that emits at a longer wavelength would be better.

Another important characteristic is the effective dynamic range as a function of intensity that impinges upon the detector. In the current embodiment, the current-to-voltage converter is designed to operate in a fixed range of current inputs set by

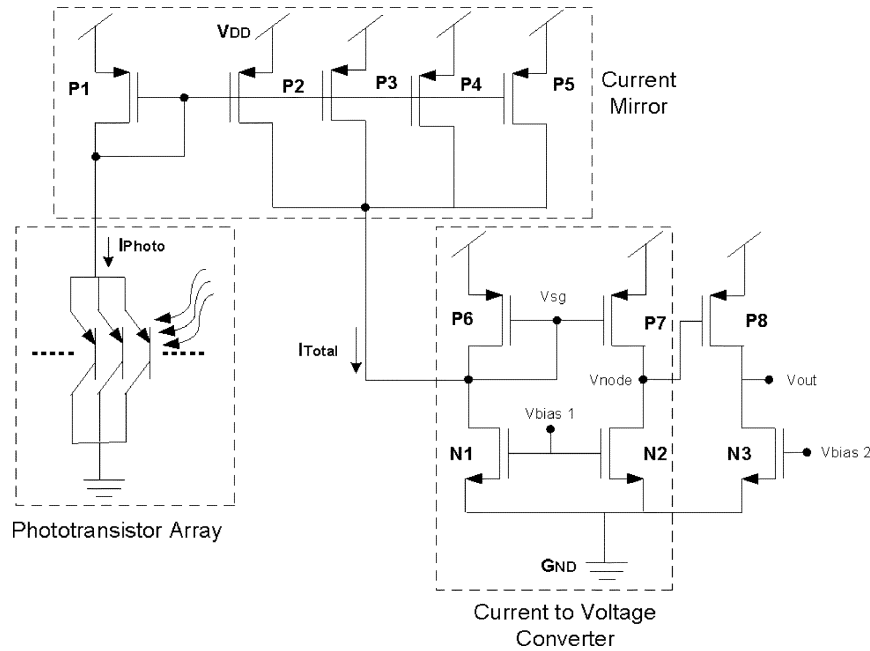


Fig. 4. Circuit diagram of the detector block.

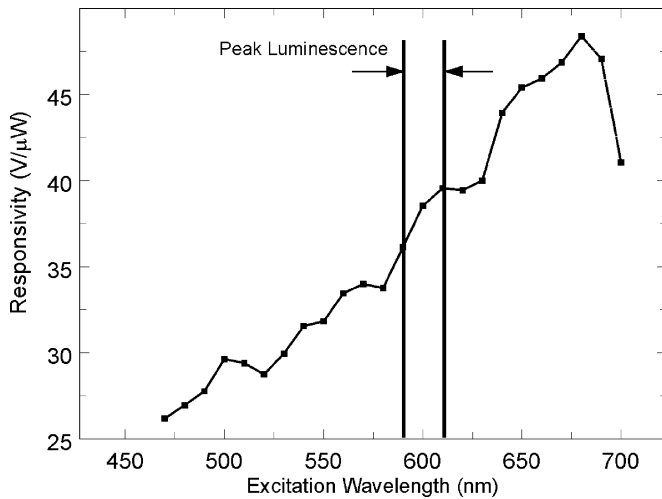


Fig. 5. Responsivity of the detector block as a function of input light wavelength.

the dimensions or aspect ratios (W/L) of the transistors P6, P7, N1, and N2. Moreover, V_{bias1} in the current-to-voltage converter must be set to an appropriate value based on the average intensity of the optical input falling on the detector. Fig. 6 shows the effects of V_{bias1} and incident beam power impinging upon the detector on the observed output voltage, V_{node} . The optical input power from a He-Ne laser (λ_{peak} : 633.2 nm, Hughes, model: 3224H-PC) is measured by using an optical power meter (Coherent, Model: Fieldmaster K538). The laser power is adjusted by using a variable transmission coefficient neutral density filter (Thorlabs, model: NDC-50C-4). From past experience, we know that the average luminescence intensity of these xerogel sensor films is between 20 and 80 nW, so based on the results shown in Fig. 6, we choose a V_{bias1} of 1.3 V.

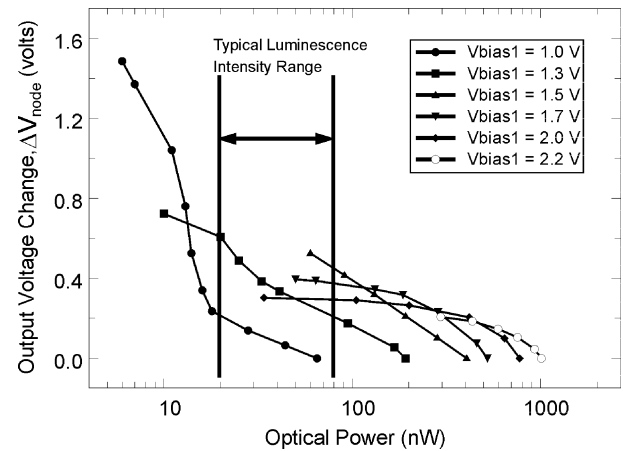


Fig. 6. Effective dynamic range of the detector block for different bias voltages.

The frequency bandwidth of the detector block is also very important especially for a modulation-based device. To verify the bandwidth of this circuit, we use a yellow LED ($\lambda_{peak} = 585$ nm, Radio Shack: 276351) as the test light source, because its optical output is similar to $[Ru(dpp)_3]^{2+}$. The LED is biased with an electrical signal that has a constant dc level of 1.5 V modulated with a 780-mV peak to peak ac component. The resulting optical power falling on the detector at all frequencies is 250 nW. Thus, we measure the voltage, V_{node} , as a function of LED modulation frequency using the value of $V_{bias1} = 1.5$ V; Fig. 7 shows this result. The exponential decrease in the voltage with increasing modulation frequency is evident; this makes clear the need for a tradeoff in the modulation frequency, which is discussed later. In the sensor system, the luminescent intensity is much lower than that used to generate Fig. 7. A lower intensity means V_{bias1} must be properly adjusted according to

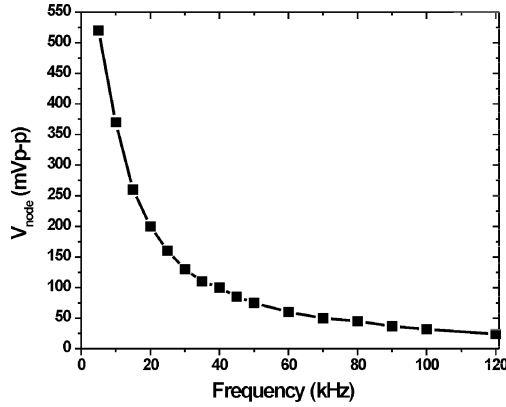


Fig. 7. Frequency response of the detector block. The peak to peak value of the voltage, V_{node} , is shown as a function of LED modulation frequency. The LED modulation signal is 780-mV peak to peak, and the incident optical power is constant at 250 nW.

Fig. 6. The curve shown in Fig. 7 is intended to show the best case frequency response for the detector block.

B. Amplifier and BandPass Filter

The current-to-voltage converter output is voltage shifted and amplified by using a standard folded cascode operational amplifier (opamp) with a gain of 10 V/V [34]. The opamp is followed by the bandpass filter, which consists of a first order high-pass stage followed by a first order low-pass stage separated by a source-follower stage [34]. The high-pass filter is formed by using a series connected external capacitor and a voltage divider acting as a parallel resistance. The low-pass filter is based on a standard g_m - C configuration using 220-pF external capacitors.

C. Phase Detector

In the final stage the bandpass filtered output is directed to a phase detector. The phase detector produces an output dc voltage that is proportional to the phase shift, θ , between the signal obtained from the phototransistor and a reference signal obtained from the function generator driving the excitation source. The phase detector consists of three stages: 1) a comparator stage; 2) an exclusive OR (XOR) stage; and 3) a low-pass filter [29], [35]. The comparator stage is implemented with a differential amplifier. Again, the low-pass filter is a g_m - C configuration using an external 1000-pF capacitor. The phase detector operates over the frequency range of 5 kHz to 1 MHz, and can respond to phase shifts between 0° and 180° with an average resolution of 25-mV/degree. A more detailed examination of the phase detector has been given elsewhere [29].

V. EXPERIMENTAL RESULTS AND DISCUSSION

Fig. 8 shows the block diagram of the sensor system and experimental test setup. It consists of a laboratory dc power supply (Instek, model: 3303) and function generator (Tektronix, model: AFG320) connected to a custom built LED driver circuit. The excitation LED ($\lambda_{peak} = 468$ nm, Radio Shack, model: 276-316) uses 5 mA with a 1.0 V (peak-to-peak) sinusoidal signal on a 2.8 V (dc) bias. The sensor response is measured as a function of gaseous O_2 concentration at room temperature

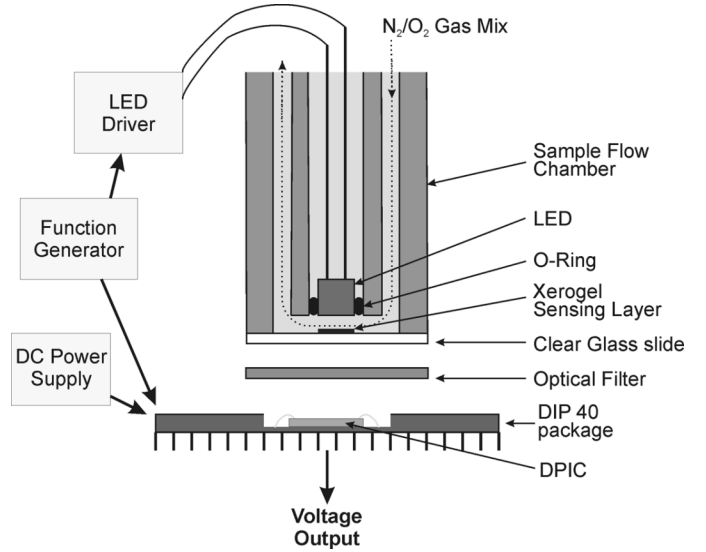


Fig. 8. Experimental setup used to test the sensor system.

(23°C). The O_2 concentration is varied by changing its relative percentage with respect to gaseous N_2 concentration. The gases are mixed within a custom built gas mixing manifold, consisting of a matched pair of flow controllers (Gilmont Instruments, model: 77701-2) connected to O_2 and N_2 gas cylinders.

In the ideal case, the Stern-Volmer plots (τ_0/τ versus $[O_2]$) for a sensor are linear [12]; however, there are numerous reasons for non-linear response profiles (e.g., a background signal arising from the luminescence from an unquenched luminophore population that are inaccessible to the oxygen and/or leakage of the excitation light through the optical filter) [26].

As shown by (2), the phase sensitivity *increases* with modulation frequency. However, as we notice from Fig. 7, the detector block voltage output *decreases* exponentially with increased frequency of modulation. Increasing the excitation source intensity is an option to address this problem; however, this causes the strength of the background signal to increase as well due to the leakage of the excitation light through the optical filter. In terms of modulation frequency, higher is better (it provides a larger phase shift). However, the higher frequencies produce a smaller node voltage (see Fig. 7). A larger output voltage swing can be achieved with a higher optical power, but we are limited by the configuration to 20–100 nW, as shown in Fig. 6. Thus, 14 kHz represents an acceptable value within these constraints.

In operation, the LED excites the $[Ru(dpp)_3]^{2+}$ -doped xerogel film. The resulting optical signal is passed through a long-pass optical filter ($\lambda_{cut-off} = 570$ nm, Melles Griot, model: OG 570) to remove the excitation radiation, and the luminescence is detected by the phototransistors within the DPIC. After the signal is processed by the DPIC, the phase detector produces a dc voltage value proportional to the phase shift between the signal obtained from the phototransistor and a reference signal obtained from the function generator. The dc voltage value is manually translated to degrees using a preset calibration for

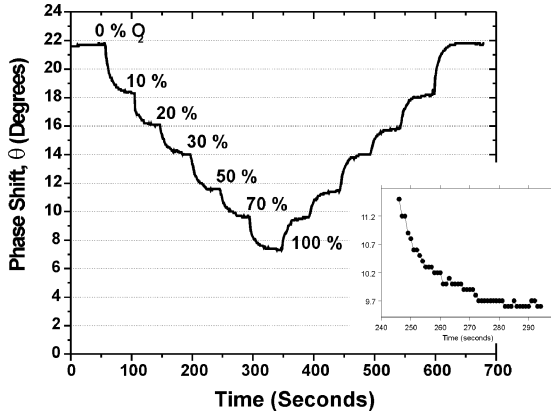


Fig. 9. Response of the sensor system for a cycle of increasing (0% to 100%) O_2 concentration and decreasing (100% to 0%) O_2 concentration. The inset shows one step from 50% to 70% O_2 .

TABLE I
COMPARISON OF PHASE SHIFTS

Reference	Circuit	Frequency	Phase Shift
[22]	Discrete Components	20kHz	14.5°
[29]	Discrete Components	20kHz	26°
This work	Integrated Circuit	14kHz	14°

the phase detector. The resulting phase shift is labeled θ_{sensor} . After this measurement, the long-pass optical filter is replaced by a short-pass optical filter ($\lambda_{\text{cut-on}} = 500$ nm, Melles Griot, model: SWP 406) and a neutral density filter to provide an excitation output comparable to the luminescence intensity and to prevent the detector from being saturated. Following the same procedure as previously described, the dc value provided by the phase detector is noted. The resulting phase shift is $\theta_{\text{excitation}}$. Thus, the phase shift proportional to the excited state lifetime (or O_2 concentration) is given by $\theta_{\text{oxygen}} = \theta_{\text{sensor}} - \theta_{\text{excitation}}$. This multistep process is required to cancel out the phase shift of the detection circuitry itself; the second step is the “dummy” measurement that is used to provide the phase information of the circuitry.

Fig. 9 illustrates the sensor response as a function of O_2 concentration. These results show that the response time is on the order of 20 s. An exponential fit to the data as the O_2 concentration increases yields an average decay time constant is -10.33 s. The results also show that the system is completely reversible, within the limits of the manual flow control valves. The curve in Fig. 9 appears to indicate that there is some hysteresis, while in fact there is none. The time required for the sensor to transition from low $[O_2]$ to high $[O_2]$ is faster than the high to low transitions, and in the experiments, the same amount of time was allotted for each transition. If the process were allowed to continue at each step of decreasing $[O_2]$, the phase angle value would saturate at the same value as that for the increasing $[O_2]$ transitions for the same $[O_2]$.

The phase angle decreases as the O_2 concentration increases as expected due to O_2 quenching [25]. Further, although the total phase shift is only 14.5° over the entire O_2 concentration range, the sensitivity and performance are comparable to results from other laboratories (see Table I).

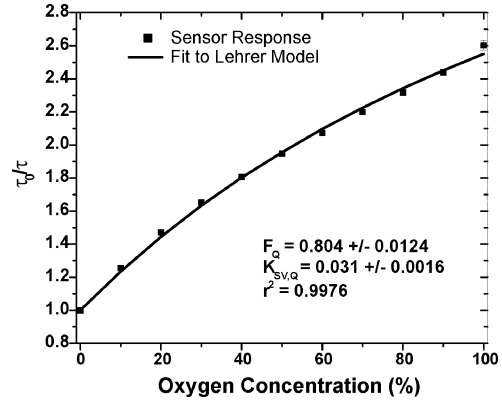


Fig. 10. Lifetime Stern–Volmer plot. F_Q is defined as the portion of the luminescent signal that is coming from the quenchable luminophores. $K_{SV,Q}$ is defined as the Stern–Volmer quenching constant for the luminophore. $1 - F_Q$ represents the background signal from the LED. Error bars represent 1 standard deviation, and are barely visible.

Fig. 10 presents the lifetime-based Stern–Volmer plot for the system. Each datum is the mean of results from multiple measurements repeated over a three week period. The lifetime measurements are obtained by measuring the phase shift obtained for different O_2 concentrations and then calculating the values for the excited state lifetimes using (2). The solid line passing through the points in the best fit to the Lehrer Model [36]. Overall, the plot shows good reproducibility. Finally, our previous analysis of these xerogel based sensors elements indicate that they are stable (reproducibility of better than 8%) for at least a year [10], [12], [37].

The complete sensor system including the LED driver operates on a 5.0-V dc power supply. For a 14-kHz modulation signal, the DPIC consumes 55 mW of average power and the LED driver consumes 25 mW of average power. Developing a completely portable hand-held instrument requires few additional off-the-shelf components. The power supply unit can be implemented using a 9.0 V battery and voltages regulators (such as KA7805 for 5.0 V dc). The function generator can be implemented using a crystal oscillator and any number of sine wave modulators or generators.

VI. CONCLUSION

We demonstrate a phase fluorometric O_2 sensor system that is based on a single-chip CMOS-based custom-designed IC for signal transduction and processing, an LED for the stimulus, and a thin film xerogel sensor. The custom-designed IC combines the photodetector and subsequent analog signal processing circuitry on a single chip.

This system operates with a single 5-V supply, which can be produced using a single 9-V battery for complete portability. We illustrate the advantages of phase fluorometric sensors and discuss the parameters that play an important role in the development of CMOS based optical sensor systems such as sensitivity, stability, and dynamic response.

The sensor system (including the gas handling equipment) has a < 400 s response time to go from 0% $[O_2]$ to 100% $[O_2]$. Note that the sensor itself responds in milliseconds, but the *system* includes all of the tubing, valves, gauges, etc., which

slows the total response time. The system is reversible, within the limit of the errors introduced by the manual operation of the flow control valves. We are currently working towards improving the signal to background noise ratio, including the LED driver circuitry on-chip to improve control and reduce power consumption, and extending the platform to other biochemical analytes such as glucose and lactate. The latter is achieved by replacing the existing O₂ sensor with a sensor that produces or uses O₂ in the presence of glucose or lactate; thus, the signal change that is measured is an indirect measurement of the analyte of interest through O₂ concentration change [38], [39].

We believe that this sensor is an important step toward the development of a fully integrated smart sensor that can detect, with high accuracy, desired analytes. The existing signal processing circuit is very compact, so multiple detectors with processing can be integrated in a single package, allowing for a large array of sensing elements. Also, combining intensity information, phase information and location information (in the array of sensors) produce significantly better results (fewer false positives and higher sensitivities), indeed leading to smarter sensors.

REFERENCES

- [1] R. Narayanaswamy and O. S. Wolfbeis, *Optical Sensors : Industrial, Environmental and Diagnostic Applications*. New York: Springer, 2004.
- [2] O. S. Wolfbeis, "Fiber-optic chemical sensors and biosensors," *Anal. Chem.*, vol. 74, pp. 2663–2677, Jun. 2002.
- [3] G. Boisdé and A. Harmer, *Chemical and Biochemical Sensing with Optical Fibers and Waveguides*. Boston, MA: Artech House, 1996.
- [4] J. R. Bacon and J. N. Demas, "Determination of oxygen concentrations by luminescence quenching of a polymer-immobilized transition-metal complex," *Anal. Chem.*, vol. 59, pp. 2780–2785, Dec. 1987.
- [5] D. M. Wilson, S. Hoyt, J. Janata, K. Booksh, and L. Obando, "Chemical sensors for portable, handheld field instruments," *IEEE Sensors J.*, vol. 1, pp. 256–274, 2001.
- [6] Y. Kostov and G. Rao, "Low-cost optical instrumentation for biomedical measurements," *Rev. Sci. Instrum.*, vol. 71, pp. 4361–4374, Dec. 2000.
- [7] A. Hierlemann, *Integrated Chemical Microsensor Systems in CMOS Technology*. New York: Springer, 2005.
- [8] E. K. Bolton, G. S. Sayler, D. E. Nivens, J. M. Rochelle, S. Ripp, and M. L. Simpson, "Integrated CMOS photodetectors and signal processing for very low-level chemical sensing with the bioluminescent bioreporter integrated circuit," *Sensors Actuat. B*, vol. 85, pp. 179–185, Jun. 2002.
- [9] E. J. Cho and F. V. Bright, "Pin-printed chemical sensor arrays for simultaneous multianalyte quantification," *Anal. Chem.*, vol. 74, pp. 1462–1466, Mar. 2002.
- [10] —, "Integrated chemical sensor array platform based on a light emitting diode, xerogel-derived sensor elements, and high-speed pin printing," *Analytica Chimica Acta*, vol. 470, pp. 101–110, Oct. 2002.
- [11] —, "Optical sensor array and integrated light source," *Anal. Chem.*, vol. 73, pp. 3289–3293, Jul. 2001.
- [12] Y. Tang, E. C. Tehan, Z. Y. Tao, and F. V. Bright, "Sol-gel-derived sensor materials that yield linear calibration plots, high sensitivity, and long-term stability," *Anal. Chem.*, vol. 75, pp. 2407–2413, May 2003.
- [13] R. M. Bukowski, R. Ciriminna, M. Pagliaro, and F. V. Bright, "High-performance quenchometric oxygen sensors based on fluorinated xerogels doped with [Ru(dpp)(3)](2+)," *Anal. Chem.*, vol. 77, pp. 2670–2672, Apr. 2005.
- [14] V. P. Chodavarapu, R. M. Bukowski, S. J. Kim, A. H. Titus, A. N. Cartwright, and F. V. Bright, "Multi-sensor system based on phase detection, an LED array, and luminophore-doped xerogels," *Electron. Lett.*, vol. 41, pp. 1031–1033, Sep. 2005.
- [15] B. D. MacCraith, C. M. McDonagh, G. Okeeffe, A. K. Mcevoy, T. Butler, and F. R. Sheridan, "Sol-Gel coatings for optical chemical sensors and biosensors," *Sensors Actuat. B*, vol. 29, pp. 51–57, Oct. 1995.
- [16] B. D. MacCraith, C. McDonagh, A. K. Mcevoy, T. Butler, G. Okeeffe, and V. Murphy, "Optical chemical sensors based on sol-gel materials: Recent advances and critical issues," *J. Sol-Gel Sci. Technol.*, vol. 8, pp. 1053–1061, 1997.
- [17] C. McDonagh, B. D. MacCraith, and A. K. Mcevoy, "Tailoring of sol-gel films for optical sensing of oxygen in gas and aqueous phase," *Anal. Chem.*, vol. 70, pp. 45–50, Jan. 1998.
- [18] A. K. Mcevoy, C. McDonagh, and B. D. MacCraith, "Optimisation of sol-gel-derived silica films for optical oxygen sensing," *J. Sol-Gel Sci. Technol.*, vol. 8, pp. 1121–1125, 1997.
- [19] C. J. Brinker and G. W. Scherer, *Sol-Gel Science : The Physics and Chemistry of Sol-Gel Processing*. San Diego, CA: Academic, 1989.
- [20] B. D. MacCraith, G. Okeeffe, C. McDonagh, and A. K. Mcevoy, "Led-based fiber optic oxygen sensor using sol-gel coating," *Electron. Lett.*, vol. 30, pp. 888–889, May 1994.
- [21] G. Okeeffe, B. D. MacCraith, A. K. Mcevoy, C. M. McDonagh, and J. F. McGilp, "Development of a Led-based phase fluorometric oxygen sensor using evanescent-wave excitation of a sol-gel immobilized dye," *Sensors Actuat. B*, vol. 29, pp. 226–230, Oct. 1995.
- [22] C. McDonagh, C. Kolle, A. K. Mcevoy, D. L. Dowling, A. A. Cafoffa, S. J. Cullen, and B. D. MacCraith, "Phase fluorometric dissolved oxygen sensor," *Sensors Actuat. B*, vol. 74, pp. 124–130, Apr. 2001.
- [23] D. Kieslinger, S. Draxler, K. Trznadel, and M. E. Lippitsch, "Lifetime-based capillary waveguide sensor instrumentation," *Sensors Actuat. B*, vol. 39, pp. 300–304, Mar.–Apr. 1997.
- [24] W. Trettnak, C. Kolle, F. Reiningner, C. Dolezal, and P. OLeary, "Miniaturized luminescence lifetime-based oxygen sensor instrumentation utilizing a phase modulation technique," *Sensors Actuat. B*, vol. 36, pp. 506–512, Oct. 1996.
- [25] J. R. Lakowicz, *Principles of Fluorescence Spectroscopy*, 2 ed. New York: Plenum, 1999.
- [26] M. Davenport, A. H. Titus, E. C. Tehan, Z. Y. Tao, Y. Tang, R. M. Bukowski, and F. V. Bright, "Chemical sensing systems using xerogel-based sensor elements and CMOS photodetectors," *IEEE Sensors J.*, vol. 4, pp. 180–188, Apr. 2004.
- [27] M. P. Davenport, A. H. Titus, E. C. Tehan, and F. V. Bright, "Chemical sensor systems using xerogels and CMOS detectors," in *Proc. 2nd IEEE Conf. Sensors*, Oct. 22–24, 2003, vol. 2, pp. 1297–1300.
- [28] M. Davenport, "Detection and processing strategies for integrated xerogel-based sensor systems," Ph.D. dissertation, Dep. Elect. Eng., The State University of New York, Buffalo, 2004.
- [29] V. P. Chodavarapu, D. O. Shubin, R. M. Bukowski, A. H. Titus, A. N. Cartwright, and F. V. Bright, "CMOS mixed-signal phase detector for integrated chemical sensor systems," in *Proc. 4th IEEE Conf. Sensors*, Oct.–Nov. 31–3, 2005, pp. 1068–1071.
- [30] C. T. Lin, W. Bottcher, M. Chou, C. Creutz, and N. Sutin, "Mechanism of quenching of emission of substituted polypyridineruthenium(II) complexes by Iron(III), chromium(III), and europium(III) ions," *J. Amer. Chem. Soc.*, vol. 98, pp. 6536–6544, 1976.
- [31] [Online]. Available: www.mosis.org
- [32] M. Fortsch, K. Schneider, and H. Zimmermann, "Simple current-to-voltage converter without stability problems," in *Proc. 2002 Int. I Semi-conductor Conf. (CAS 2002)*, 2002, vol. 1, pp. 181–184.
- [33] S. M. Sze, *Physics of Semiconductor Devices*. New York: Wiley, 1981.
- [34] R. J. Baker, H. W. Li, and D. E. Boyce, *CMOS Circuit Design, Layout, and Simulation*. New York: Wiley-IEEE Press, 1997.
- [35] B. Razavi, *Design of Analog CMOS Integrated Circuits*. New York: McGraw-Hill, 2001.
- [36] E. R. Carraway, J. N. Demas, and B. A. Degraff, "Luminescence quenching mechanism for microheterogeneous systems," *Anal. Chem.*, vol. 63, pp. 332–336, Feb. 1991.
- [37] E. Cho, Z. Tao, E. Tehan, and F. Bright, "Multianalyte pin-printed biosensor arrays based on protein-doped xerogels," *Anal. Chem.*, vol. 74, pp. 6177–6184, 2002.
- [38] J. C. Pickup, F. Hussain, N. D. Evans, O. J. Rolinski, and D. J. S. Birch, "Fluorescence-based glucose sensors," *Biosensors Bioelectron.*, vol. 20, pp. 2555–2565, 2005.
- [39] X. J. Wu, M. M. F. Choi, and D. Xiao, "A glucose biosensor with enzyme-entrapped sol-gel and an oxygen-sensitive optode membrane," *Analyst*, vol. 125, pp. 157–162, 2000.



Vamsy P. Chodavarapu (S'03) received the B.E. degree in instrumentation engineering from Osmania University, Hyderabad, India, in 2001, and the M.S. and Ph.D. degrees in electrical engineering from the University at Buffalo, The State University of New York, Buffalo, in 2003 and 2006, respectively.

Currently, he is an Assistant Professor in the Department of Electrical and Computer Engineering at McGill University, Montreal, QC, Canada. His research interests are CMOS sensor microsystems, microfabrication technologies, and mixed-signal VLSI.

Daniil O. Shubin received the B.S. and M.S. degrees in electrical engineering from the University at Buffalo (UB), State University of New York, Buffalo in 2004 and 2006, respectively.

Currently, he is a Test Engineer in the Micro and Nano Structures Technology (MNST) Department of General Electric Global Research, Niskayuna, New York. His research interests include MEMS, system-on-chip sensors and mixed-signal VLSI.



Rachel M. Bukowski received the B.S. degree in chemistry from Union College, Schenectady, NY, in 2002. She is currently pursuing the Ph.D. degree in analytical chemistry at the University at Buffalo, The State University of New York, Buffalo.

Her research interests include protein biosensor fabrication on a xerogel platform.



Albert H. Titus (S'86–M'97) received the B.S. and M.S. degrees from the University at Buffalo (UB), The State University of New York, Buffalo, in 1989 and 1991, respectively, and the Ph.D. degree from the Georgia Institute of Technology, Atlanta, in 1997.

He is an Assistant Professor in the Department of Electrical Engineering, UB. Prior to joining the faculty at UB, he was an Assistant Professor at the Rochester Institute of Technology, Rochester, NY. His research interests include analog VLSI implementations of artificial vision, hardware and software

artificial neural networks, hardware implementations of decision-making aids, optoelectronics and integrated sensor systems.

Dr. Titus has numerous research grants from federal and private sources, including an NSF CAREER award. He has been a reviewer for many journals and conferences, and, he is a member of IEEE, INNS, ASEE and SPIE.



Alexander N. Cartwright (M'95) received the B.S. and Ph.D. degrees in electrical and computer engineering from the University of Iowa, Iowa City, Iowa.

He is an Associate Professor of Electrical Engineering, Director of the Institute for Lasers, Photonics and Biophotonics at the University at Buffalo (UB), The State University of New York, Buffalo, and Co-Director of the Electronics Packaging Laboratory at the UB. His research is focused on III-Nitride materials, quantum dot materials, optical non-destructive testing of stress and strain

for device reliability, optical sensors, biophotonics, nanophotonics and nano-electronics.

Dr. Cartwright received a NSF CAREER Award, in 1998, and in 2000, a Department of Defense Young Investigator Award for research on optical properties of III-Nitride materials. More recently, he was the recipient of the 2002 State University of New York's Chancellor's Award for Excellence in Teaching.



Frank V. Bright received the B.S. degree in chemistry from the University of Redlands, Redlands, CA, and the Ph.D. degree in chemistry from Oklahoma State University, Oklahoma City.

He was a postdoctoral associate at Indiana University, Bloomington. He is a UB Distinguished Professor of Chemistry, holder of the A. Conger Goodyear Chair of Chemistry, and the Associate Chairperson in the Department of Chemistry, University at Buffalo, The State University of New York, Buffalo. His research interests include biosensing,

biomaterials, environmentally friendly solvent systems, chemical analysis of things as they are, and chemical instrumentation. He has over 200 publications and five issued U.S. patents.

Dr. Bright is currently a member of the following editorial boards: *Applied Spectroscopy*, *Analytica Chimica Acta*, and *Journal of Fluorescence*. He has received several awards, including a 3M, Inc. Non-tenured Faculty Award, UB Faculty of Natural Sciences and Mathematics Award for Excellence in Teaching, Eastern New York Section of the American Chemical Society Buck-Whitney Medal, State University of New York Chancellor's Award for Excellence in Teaching, State University of New York Outstanding Inventors Award, New York Section of the Society for Applied Spectroscopy Gold Medal, and the Akron Section of the American Chemical Society Award.